Photoluminescence of inversion electrons with carbon acceptors in a single modulation-doped $Al_xGa_{1-x}As/GaAs$ heterostructure

J. Schuster, T. Y. Kim, and E. Batke*
Physikalisches Institut der Universität Würzburg, Am Hubland, D-97074 Würzburg, Germany

D. Reuter and A. D. Wieck
Lehrstuhl für Angewandte Festkörperphysik, Ruhr-Universität Bochum, Universitätsstraße 150, D-44780 Bochum, Germany
(Received 24 October 2012; revised manuscript received 20 December 2012; published 30 January 2013)

The photoluminescence of inversion electrons with carbon acceptors in a modulation-doped $Al_xGa_{1-x}As$-GaAs single heterostructure was studied for different temperatures and excitation intensities. Despite the essentially homogeneous distribution of residual acceptors in the GaAs buffer, well-resolved luminescence profiles are observed for the ground and first excited two-dimensional electron subbands. This is due to the fact that the inversion layer interface potential restricts the overlap of the electron and acceptor wave functions to limited spatial regions close to the $Al_xGa_{1-x}As$-GaAs interface, where the transition energies are weakly dispersive. A simple model will be presented for the calculation of the luminescence line shape that allows a quantitative analysis of the experiment.

DOI: 10.1103/PhysRevB.87.035433 PACS number(s): 78.55.Cr, 73.20.Hb, 73.40.Kp, 78.67.Pt

I. INTRODUCTION

Introducing a δ doping of acceptors in the buffer of an $Al_xGa_{1-x}As$-GaAs single heterostructures is a well established and widely used approach in the investigation of electron inversion layer properties.[1,2] This is due to the fact that a sufficiently localized acceptor breaks the $\vec{k}$-selection rule, and nearly all populated two-dimensional (2D) wave vectors can contribute to the photoluminescence (PL) line. Nevertheless, the δ doping constitutes a perturbation to the 2D system, since it introduces additional charged scatterers close to the inversion layer, possibly degrading the mobility. Furthermore, the δ doping alters the interface electric potential compared to the undoped situation with consequences for the inversion electron subband quantization and population.[2] Avoiding those complications, one would like to test inversion layer properties in usual heterostructures.

It will be demonstrated that one can come closest to the bare inversion layer properties via radiative recombination to the residual background doping of the GaAs buffer. This approach also benefits from the breaking of the $\vec{k}$-selection rule and can be advantageously applied in principle to any properly grown single heterostructure with a p-doped buffer. Since the background doping can be assumed to be distributed homogeneously in the buffer, one could expect that radiative transitions are strongly dispersed in energy space such that well-defined PL lines might not be observable. Contrary to this suspicion, we found well-resolved resonances from the ground and first excited 2D electron subbands with the unintentional carbon buffer doping in $Al_xGa_{1-x}As$-GaAs single heterostructures. We studied the PL depending on excitation intensity and temperature, and we provide a simple model for the PL line shapes.

II. EXPERIMENT

Our $Al_{0.35}Ga_{0.65}As$-GaAs samples were grown on semi-insulating (100) GaAs substrate and have the same layer sequence as the samples with setback doping investigated previously.[2] Magnetotransport investigations performed on Hall bars at 4.2 K in the dark reveal a surface electron density $N_S = (1.5 \pm 0.1) \times 10^{11}$ cm^{-2} and a mobility $\mu \approx 4.0 \times 10^5$ cm^2 V^{-1} s^{-1}. After illumination with a short pulse of a 635 nm laser diode, the density increases to $N_S = (4.0 \pm 0.2) \times 10^{11}$ cm^{-2} and the mobility to $\mu \approx 1.1 \times 10^6$ cm^2 V^{-1} s^{-1}, indicating a strong persistent photoeffect.

The experiment was performed with a 0.275 m monochromator and a photon counting system equipped with a Si avalanche photodiode. All samples were mounted strain-free in a helium bath cryostat with a superconducting magnet and cooled by He-exchange gas to liquid helium temperatures. Via a controller, sample temperatures in excess of 4.2 K could be achieved. A bundle of 80 μm diameter fibers served to guide the light. Excitation light of a laser diode (typically 3–4 mW) was focused into a single fiber statistically distributed in the bundle. The scattered and reflected light was collected by about 40 fibers and mapped to the entrance slit of the monochromator. Laser light reflected from a 780 nm scatter filter in front of the slit was used to stabilize the laser diode intensity via a proportional-integral-derivative (PID) controller and a Si photodiode. The laser intensity could be varied with voltage and/or calibrated metal absorption filters. The experimental setup was calibrated with a krypton lamp to an accuracy and resolution of about 0.1 and 0.2 meV, respectively.[3]

III. RESULTS AND DISCUSSION

A. Experimental spectra

In Fig. 1, the PL is shown for a laser wavelength of 635 nm at various illumination intensities in the energy regime 1.47–1.51 eV. The response is dominated by the PL transitions from the ground ($i = 0$) and first excited ($i = 1$) 2D subbands. Above about 1.504 eV, bulk exciton transitions dominate. The profile of the $i = 1$ subband is a nearly symmetric resonance-type line, whereas that of the ground subband approaches a hat-shaped form with increasing illumination. With enhanced illumination, various bulk transitions gain in

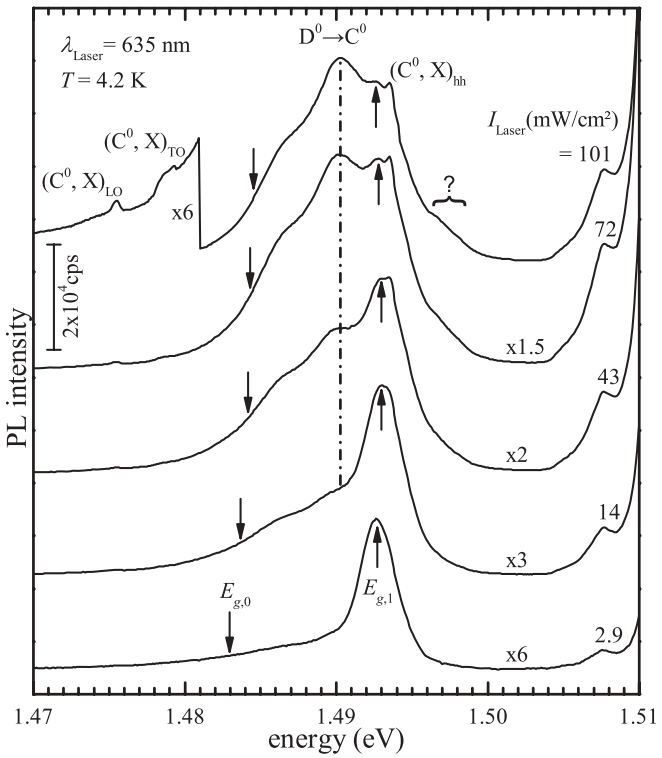

FIG. 1. PL of a GaAs single heterostructure for different illuminations I_{laser} ($\lambda_L = 635$ nm) at 4.2 K. Measurements at lower illumination are amplified as indicated. Downward and upward pointing arrows indicate, respectively, the photoluminescence gaps $E_{g,0}$ and $E_{g,1}$ of the ground and first excited 2D subbands. The dashed-dotted line marks the position of a GaAs bulk donator to carbon acceptor transition. Weaker bulk contributions associated with the carbon acceptor bound exciton are a LO phonon $(C^0,X)_{\text{LO}}$ and a two-hole replica $(C^0,X)_{\text{hh}}$. $(C^0,X)_{\text{TO}}$ is presumably a TO phonon replica and a spectral structure marked ? is in question.

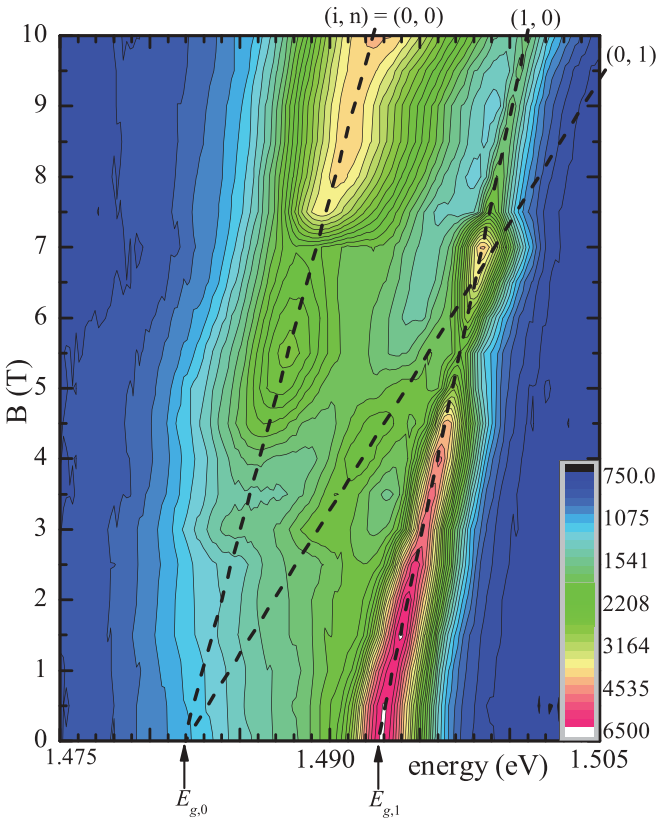

FIG. 2. (Color online) Magnetoluminescence contour plot for illumination $I_{\text{laser}} = 8$ mW/cm^2. The dashed lines are guides to the eye and indicate subband Landau levels $(i,n = 0,1)$ for the 2D subbands $i = 0$ and 1. Extrapolation to the limit $B = 0$ yields the subband gaps $E_{g,0}$ and $E_{g,1}$.

strength. The dominating one is a donator to carbon acceptor transition $D^0 \rightarrow C^0$ at ≈ 1.490 eV.[4] Weaker contributions arise from a ongitudinal optical (LO) phonon[5] and two-hole replicas[6] of the carbon acceptor bound exciton (C^0,X).

The downward and upward pointing arrows indicate, respectively, the positions of the ground and first excited PL-subband gaps $E_{g,0}$ and $E_{g,1}$. The gap positions were determined from magneto-optical investigations in Faraday geometry in magnetic fields up to 10 T. The PL gap for the ground subband increases slightly with increasing illumination (see Fig. 1), whereas the edge of the first excited subband remains essentially constant. This observation agrees qualitatively with the one for setback δ-doped samples, which exhibit a negative photoeffect, i.e., a reduced 2D electron concentration dependent on excitation laser wavelength and intensity.[7]

In Fig. 2, a contour plot is shown exemplarily for a small illumination intensity $I_{\text{laser}} \approx 8$ meV. The dashed lines indicate subband Landau levels $(i,n = 0,1)$. Extrapolation to the limit $B = 0$ defines the PL-subband gaps. Obviously, $E_{g,1}$ is identical to the maximum of the experimental profile. A good approximation to $E_{g,0}$ is obtained if one takes the lower edge position of the full width at half-maximum of the ground subband PL. Two Landau levels are clearly resolved for the ground subband, with only one Landau level present for the $i = 1$ subband. This provides clear evidence that a degenerate electron system is present and that the electron inversion layer is in a quasielectric quantum limit, with the $i = 1$ subband only weakly populated. The difference of the PL subband gaps $E_{g,1} - E_{g,0}$, which is 11 meV at lower illuminations, provides an estimate of the electron Fermi energy $E_{F,e}$. With an electron effective mass of $m^* = 0.067m_e$, this value gives a ground subband density of 3.1×10^{11} cm^{-2}. Note that there is an oscillatory behavior of the magnetoluminescence with magnetic field strength B, e.g., there is a minimum in the luminescence yield around 7 T for the ground subband. This is very close to a filling factor of 2 if a density of 3.1×10^{11} cm^{-2} is considered. The filling factor dependence clearly demonstrates that we deal here with 2D and not bulk properties. A more detailed consideration of the magnetoluminescence aspects will be given elsewhere.[8]

Figure 3 exhibits the temperature dependence of the PL for medium illumination. With increasing temperature the PL rapidly diminishes, and the integrated strength of the ground subband degrades more rapidly compared to the strength of the $i = 1$ subband. Both observations are in agreement with an enhanced population of the first excited at the expense of the ground subband. A higher population of the $i = 1$ subband enhances the interface potential pushing the inversion electrons closer to the interface. Consequently, the overlap

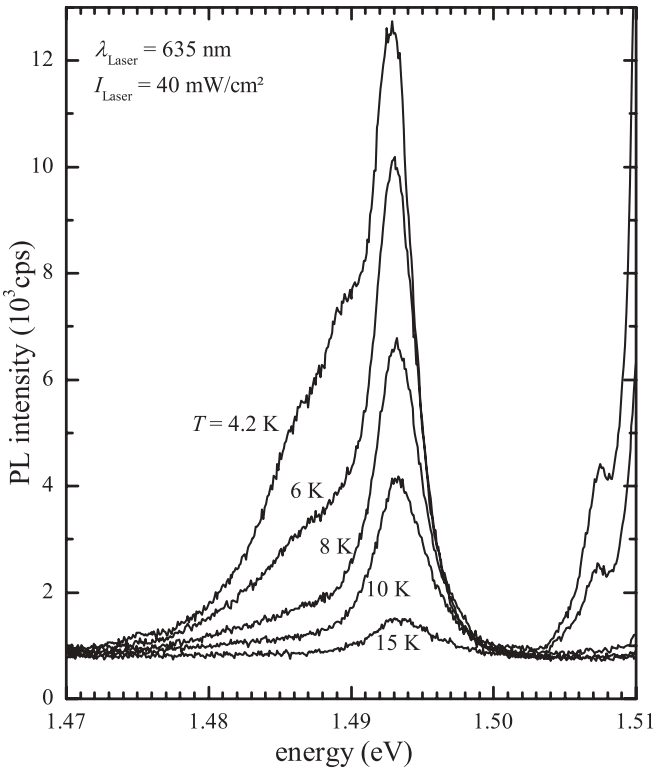

FIG. 3. Dependence of the luminescence on lattice temperature T.

with the neutral acceptors existing in deeper regions of the buffer decreases and reduces the PL yield. The PL from the $i = 1$ subband survives at higher temperatures since its wave function extends more deeply in the buffer.

B. Calculated PL line shape

For a deeper understanding of what controls the PL, we performed a line-shape calculation. The background of the calculation is depicted in Fig. 4. The band bendings $E_{v(c)}(z > 0) - E_{v(c)}(0)$ represent the potential $V(z)$ that governs the 2D subband bottom energies E_i $(i = 0,1)$. The potential $V(z)$ depends on the electron interface charge densities $N_{S,i}$ in the subbands i and the distribution of ionized acceptors N_A^- and donors N_D^+ in the GaAs buffer. The PL transition energies depend on the acceptor position z in the GaAs buffer and the 2D wave vector $\vec{k}$ parallel to the interface. For an isolated acceptor with binding energy E_A relative to the valence band edge, one obtains in a single-particle approximation

$$h\nu_i(\vec{k},z) = E_g + E_i - V(z) - E_A + \frac{\hbar^2\vec{k}^2}{2m^*} = E_{g,i}(z) + \frac{\hbar^2\vec{k}^2}{2m^*}. \quad (1)$$

The PL edges $E_{g,i}(z)$ depend of the position z in the growth direction via the interface potential $V(z)$ and are governed by the bulk GaAs gap E_g, the 2D subband energies E_i, and the acceptor binding energy E_A. Transitions from electrons populating the kinetic energy states $E_{\rm kin} = \hbar^2\vec{k}^2/2m^*$ to the distribution of neutral acceptors $N_C^0(z)$ in the GaAs buffer yield the PL line. For an electron inversion layer in thermal equilibrium, the PL line for subband i is calculated from the

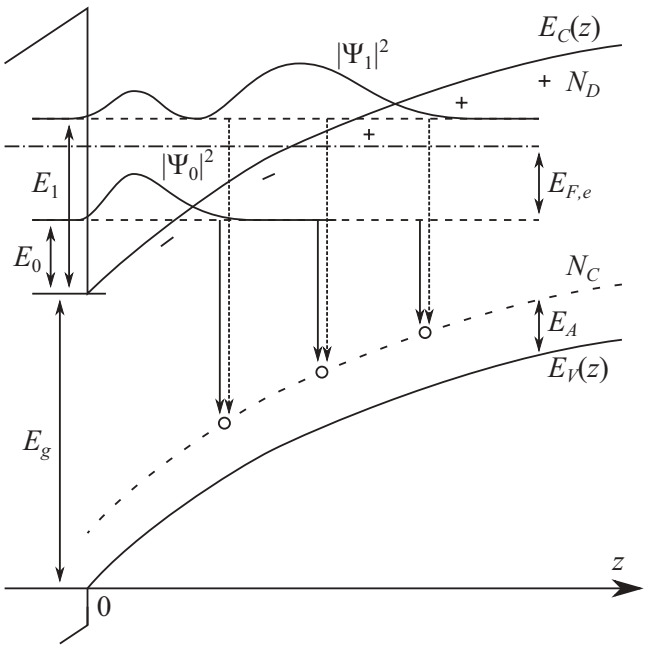

FIG. 4. Schematic picture of the conduction $E_c(z)$ and valence band edges $E_v(z)$ for a GaAs heterostructures in growth direction z. The point of zero energy is set to $E_v(0)$. E_g, E_0 $[|\Psi_0(z)|^2]$, E_1 $[|\Psi_1(z)|^2]$, $E_{F,e}$, E_A, N_C, and N_D indicate, respectively, the bulk GaAs fundamental gap, the ground and first excited subband bottom energies (probability densities), the electron Fermi energy, the acceptor binding energy, and the background acceptor and donator doping concentrations. The downward pointing arrows indicate PL transitions from the $i = 0$ and 1 2D subbands to neutral acceptors in the GaAs buffer.

expression

$$I_i(h\nu) = A\int_0^\infty N_C^0(z)\,\mathrm{erfc}\left(\frac{E_{g,i}(z) - h\nu}{\sqrt{2}\sigma_i}\right) \times M_i[h\nu - E_{g,i}(z),z]\frac{1}{e^{\frac{h\nu - E_{g,0}(z) - E_F}{k_B T_e}} + 1}\,dz, \quad (2)$$

where A is a scaling parameter, T_e is an effective electron temperature, $\mathrm{erfc}(x)$ is the complementary error function, $M_i(E_{\rm kin},z)$ is a transition strength depending on the spatial extents of the 2D electron and the acceptor wave functions,[9] and σ_i is a subband specific parameter accounting for a Gaussian fluctuation of the subband bottom energy. For a bulk-type acceptor, a very good approximation of the transition strength is given by $M_i(E_{\rm kin},z) \approx |\Psi_i(z)|^2(1 - m_i E_{\rm kin})$,[3] where the quantity m_i is essentially a constant.

The key quantities in the evaluation of Eq. (2) are the interface potential $V(z)$ and the distribution of neutral acceptors $N_C^0(z)$. The question arises whether the distribution of neutral and ionized acceptors is close to an equilibrium form and can be described by a hole Fermi energy $E_{F,h}$ and an associated hole temperature T_h. This is not obvious; however, we will show below that this working hypothesis provides a surprisingly good agreement with the experiment.

The calculation of the 2D subband structure is performed self-consistently taking into account a homogeneous

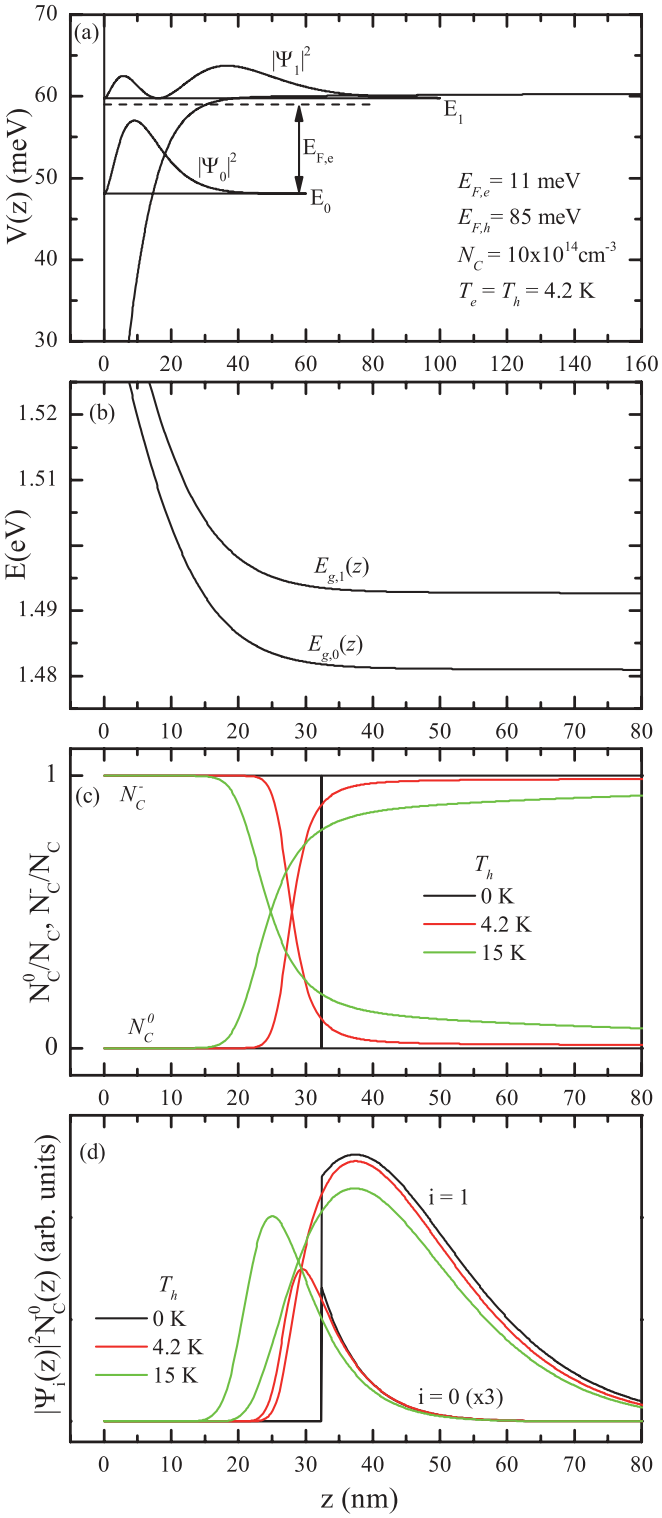

FIG. 5. (Color online) Calculated subband and PL properties for a GaAs heterostructure under illumination. Fixed Fermi energies $E_{F,e}$ and $E_{F,h}$, background doping concentration N_C, and temperatures T_e and T_h were assumed. (a) Interface potential $V(z)$ with subband energies and squared wave functions. (b) Position dependence of the PL subband edges $E_{g,i}(z)$. (c) Normalized neutral and ionized acceptor distributions for different hole temperatures T_h. (d) Position-dependent luminescence yield for different hole temperatures T_h.

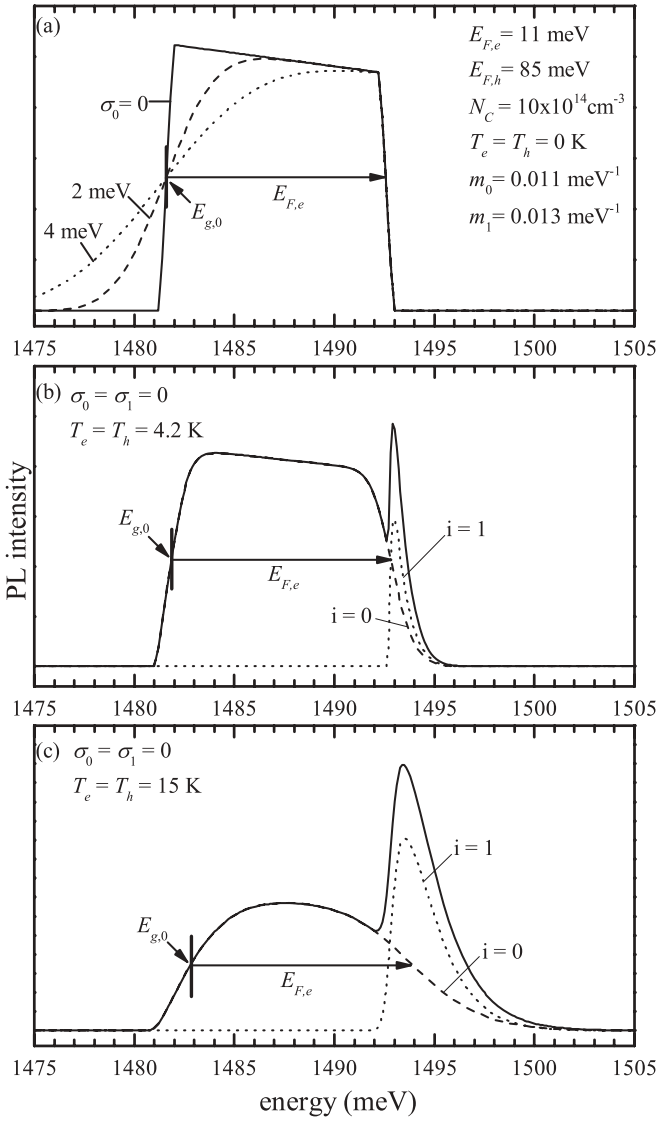

FIG. 6. Calculated temperature-dependent 2D PL line shapes assuming the parameters of Fig. 5. (a) Ground subband PL at temperatures $T_e = T_h = 0$ for different broadening parameters σ_0. The horizontal arrow indicates the electron Fermi energy and the small bold vertical line marks the ground subband PL gap $E_{g,0}$. (b) Finite temperatures $T_e = T_h = 4.2$ K and zero broadening $\sigma_0 = \sigma_1 = 0$. (c) Same as (b) but for elevated temperatures $T_e = T_h = 15$ K.

carbon-doping N_C of the GaAs buffer. Image influences and many-body contributions are neglected because they are of minor importance. Self-consistency is accomplished by a simultaneous solution of the Schrödinger and Poisson equations,

$$-\frac{\hbar^2}{2m^*}\frac{d^2\psi_i(z)}{dz^2} + V_1(z)\psi_i(z) = E_i\psi_i(z), \tag{3}$$

$$\frac{d^2V_j(z)}{dz^2} = -\frac{e^2}{\epsilon_s\epsilon_0}\left(N_C^-(z) + \frac{N_{S0}}{j}|\Psi_0(z)|^2\right) \tag{4}$$

for the 2D envelope functions $\Psi_i(z)$ and the potentials $V_j(z)$ ($j = 1,2$). The distribution of the ionized carbon atoms is

calculated from

$$N_C^-(z) = \frac{N_C}{1 + g_A e^{\frac{V_1(z)+E_A-E_{F,h}}{k_B T_h}}}, \quad (5)$$

assuming a monovalent acceptor with degeneracy factor $g_A = 4$. We treat here only the electric quantum limit, and a small charge in the higher subbands will be neglected. The set of Eqs. (3)–(5) is solved variationally with orthonormalized test wave functions of Fang-Howard type $\Psi_0(z) = \sqrt{\frac{b_0^3}{2}} z e^{-\frac{b_0 z}{2}}$ and $\Psi_1(z) = \sqrt{\frac{3b_1^3}{2}} \sqrt{\frac{b_1^2}{b_0^2 - b_0 b_1 + b_1^2}} z(1 - \frac{b_0+b_1}{6} z) e^{-\frac{b_1 z}{2}}$. With $z = 0$ set at the interface, we apply the boundary conditions $V_m(0) = 0$ and $\frac{dV_m(z)}{dz}|z = z_{\text{buffer}} = 0$. With the potentials Eq. (4), the subband properties can be calculated along the lines described in Ref. 10. For given $E_{F,e}$ and N_C, the hole Fermi energy $E_{F,h}$ is varied to obtain the best agreement with the PL subband gaps and the integrated subband strengths.

In Fig. 5, we present calculated subband and PL properties for fixed electron $E_{F,e}$ and hole $E_{F,h}$ Fermi energies, background doping concentration N_C, and equal electron T_e and hole T_h temperatures. Figure 5(a) shows part of the interface potential, the subband energies E_0 and E_1, and the squared wave functions $|\Psi_0(z)|^2$ and $|\Psi_1(z)|^2$. Part (b) depicts position-dependent PL edges $E_{g,i}(z)$, and in (c) the distribution of ionized and neutral acceptors for different hole temperatures T_h was calculated from Eq. (5) and $N_C^0(z) = N_C - N_C^-(z)$. The depth-dependent luminescence yield is shown in Fig. 5(d). Due to the interplay of the decreasing wave functions and the increasing neutral acceptor concentration with buffer depth, the spatial region for optimum luminescence yield is limited to a spatial region ranging from 20 to about 70 nm. Note that the maxima, i.e., the positions of optimum PL yield for the ground and the first excited subbands, are located at different depths in the buffer $z_{0,\max}$ and $z_{1,\max}$, respectively.

Predicted PL profiles assuming the parameters of Fig. 5 are shown in Fig. 6. The calculation was performed for equal but varying temperatures $T_e = T_h$. Figure 6(a) depicts the electric quantum limit $T_e = T_h = 0$ with only the ground subband populated for different broadenings σ_0. For $\sigma_0 = 0$, the PL line is hat-shaped. The lower edge defines the PL subband gap $E_{g,0}$ and the higher edge defines the Fermi edge. This seems surprising at first glance in view of the spatial distribution of the luminescence yield, Fig. 5(d). However, this distribution is not effective in broadening the PL line since the transitions are restricted to positions $z \gtrsim 30$ nm where the edge energy $E_{g,0}(z)$ [see Fig. 5(b)] saturates. The electron Fermi energy $E_{F,e}$ can be estimated from the full width at half-maximum of the PL profile. This is not an exact measure; however, it provides an accuracy of the order of 1 meV, even in the case of higher temperatures and larger broadenings, σ_0. Note that with increasing broadening the lower edge of the PL profile strongly weakens. At higher temperatures, the distribution of luminescence yield shifts to small z values as is shown Fig. 5(d) and the first excited 2D subband becomes populated. Thus, the PL line edge of the ground subband weakens due to the stronger spatial variation of $E_{g,0}(z)$ and the first excited subband contributes with a resonance type line at the Fermi edge of the ground subband [Fig. 6(b)]. With further enhanced temperature, as shown in Fig. 6(c), the lines of both subbands broaden and the first excited subband gains in strength at the expense of the ground subband. Note that due to $z_{0,\max} < z_{1,\max}$, the PL lines from both 2D subbands have an enhanced overlap compared to δ-doped samples. This overlap limits somewhat a straightforward determination of subband separations from the experimental spectra.

The calculated PL lines reflect the major experimental observations and support the assumptions. The background doping level cannot be exactly fixed. However, satisfactory agreement between calculation and experiment is only obtained for the interval 5×10^{14} cm$^{-3} \lesssim N_C \lesssim 10 \times 10^{14}$ cm^{-3}. Generally, with reduced doping level, the position of optimum luminescence yield shifts to deeper regions of the GaAs buffer.

IV. SUMMARY

In conclusion, we studied the PL from an electron inversion layers to the unintentional carbon-doping in GaAs. Well-resolved PL profiles were observed for the ground and the first excited 2D subbands, demonstrating that the transitions occur in limited spatial regions close to the interface with very similar energies. The PL profiles were calculated in the framework of a model assuming an equilibrium hole distribution that provides a surprisingly good agreement with the experiment.

*batke@physik.uni-wuerzburg.de

[1] I. V. Kukushkin and V. B. Timofeev, Adv. Phys. **45**, 147 (1996).
[2] J. Schuster, T. Y. Kim, E. Batke, D. Reuter, and A. D. Wieck, J. Phys.: Condens. Matter **24**, 165801 (2012).
[3] J. Schuster, T. Y. Kim, E. Batke, D. Reuter, and A. D. Wieck (unpublished).
[4] B. J. Skromme and G. E. Stillman, Phys. Rev. B **29**, 1982 (1984).
[5] C. Hartmann, G. Martinez, C. A. Fisher, D. W. Braun, and K. Ploog, Europhys. Lett. **41**, 559 (1998).
[6] D. J. Ashen, P. J. Dean, D. T. J. Hurle, J. B. Mullin, A. M. White, and P. D. Greene, J. Phys. Chem. Solids **36**, 1041 (1975).
[7] M. S. Skolnick, C. W. Tu, and T. D. Harris, Phys. Rev. B **33**, 8468 (1986).
[8] J. Schuster, T. Y. Kim, E. Batke, D. Reuter, and A. D. Wieck (unpublished).
[9] J. Łusakowski, R. Buczko, K.-J. Friedland, and R. Hey, Phys. Rev. B **83**, 245313 (2011).
[10] T. Ando, A. B. Fowler, and F. Stern, Rev. Mod. Phys. **54**, 437 (1982).